Radio Imaging by Cooperative Wireless Network: Localization Algorithms and Experiments

Stefano Savazzi, Monica Nicoli, Michele Riva
Dip. di Elettronica e Informazione, Politecnico di Milano, Italy. E-mail: (savazzi, nicoli)@elet.polimi.it

***Abstract*— Radio imaging allows to locate and track passive targets (i.e., not carrying electronic device) moving in an area monitored by a dense network of low-power and battery-operated wireless sensors. The technology is promising for a wide number of applications ranging from intrusion detection to emergency and rescue operations in critical areas. In this paper, a new approach is proposed where *both* the average *and* the variance of the fluctuations of the received signal strength (RSS) induced by the target movement over the links are jointly and optimally exploited for sensing the target location. A link-layer protocol is developed on top of an existing IEEE 802.15.4 compliant PHY/MAC layer to allow the wireless nodes to cooperatively exchange RSS measurements. A log-normal model is defined to relate these measurements to the target location. Grid-based Bayesian estimation is proposed for real-time mobile positioning. The proposed system is validated by an indoor experimental study that analyzes the problem of model calibration and compares the performance of different localization algorithms.**

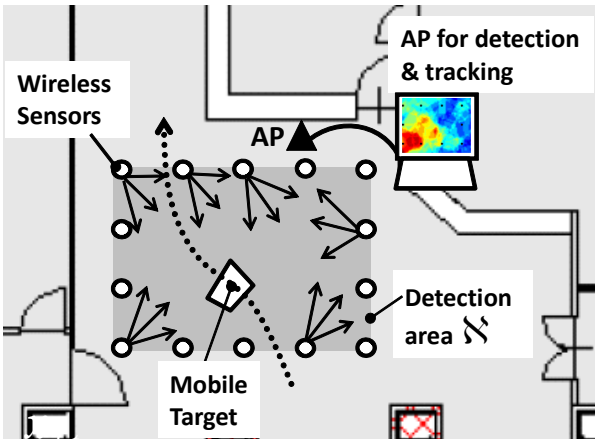

Fig. 1. Radio imaging system: floor map and WSN layout.

I. Introduction

Radio Imaging is an emerging technology for locating and tracking moving objects or people in areas that are monitored by simple low-cost radios. Conventional indoor positioning techniques require the device being tracked to actively participate in the localization process [1], while radio imaging does not require the target to carry any electronic equipment thus enabling device-free (*passive*) localization [2]. In contrast to well-known ultra-wide band based imaging techniques [3], radio imaging relies on inexpensive commercial radios that have small bandwidth and provide only signal strength measurements (rather than reflections or scattering). As depicted in Fig. 1, a large set of small, low-power and battery-operated wireless devices is spread over the area of interest creating a dense mesh network. An object that moves within the area modifies the received signal strength (RSS) field in a way that depends on the object locations; radio imaging therefore exploits RSS measurements observed along the peer-to-peer links to obtain an image reconstruction of the object trajectory.

Radio imaging is promising for a wide number of applications ranging from intrusion detection to emergency and rescue operations in critical or hazardous areas, access control and counting, pedestrian traffic monitoring and home automation. Still, there are a number of technical challenges that need to be addressed. These include the definition of reliable statistical models (and related calibration procedures) to describe the impact of the attenuating/diffracting/scattering target on the RSS measurements, as well as the design of efficient mobile positioning algorithms and networking protocols for real-time applications. A step forward in this direction is done in [4] with the proposal of a tomographic method for radio imaging with narrowband devices: localization is based on a geometrical deterministic model to describe attenuation changes over the space, while an image estimate is performed to indicate the position of the moving object. In this paper, radio imaging is cast into a new Bayesian estimation framework based on a stochastic model that allows to optimally exploit all the location information coming from attenuation, random fading and mobility model.

The proposed radio-imaging system is based on a link-layer protocol that allows the nodes to cooperatively exchange RSS measurements. The protocol has been developed on top of an existing IEEE 802.15.4 compliant physical/medium-access-control (PHY/MAC) layer design. A stochastic model is proposed for relating the RSS measurements of each link to the object position: since the presence of the target is shown to affect both the path loss and the degree of random fluctuation, a log-normal model is defined where the RSS mean and variance are functions of the target location. The model is calibrated on experimental data. For positioning, multi-link measurements are optimally combined in a multi-angulation like fashion. We compare maximum likelihood estimation (MLE) without tracking with a more advanced Bayesian on-line sequential estimation that exploits a priori information on the target mobility to alleviate false localization problems [8]. Preliminary results from test-bed measurements confirm that the proposed model provides a reliable description of RSS changes caused by moving objects and allows to obtain good

978-1-4673-0437-5/12/$31.00 ©2012 IEEE

localization performance. In addition, the use of a cooperative network architecture for real-time sampling of the RSS field is shown to provide a practical network architecture for on-line target detection and tracking.

II. Problem Formulation

We consider a wireless sensor network (WSN) spread in an indoor planar region $\mathcal{X} \subset \mathbb{R}^2$ where N wireless sensors (WS) are allowed to share transmission resources to communicate with an access point (AP). $\mathcal{X}$ is the coverage area of the WSN. Sensor i-th ($i = 1, \ldots, N$) is placed in a known position $\mathbf{z}_i = [z_{1,i}, z_{2,i}] \in \mathcal{X}$, where $z_{k,i}$ denotes the $k-$th Cartesian coordinate ($k = 1, 2$) in the two-dimensional (2D) space. These known positions can be either measured during the deployment or estimated by the WSN itself by using a cooperative localization algorithm [1]. We model the WSN as an unidirectional connected graph with wireless links (edges) indexed by $\ell \in \mathcal{L} = \{1, \ldots, L\}$. $\mathcal{L}$ denotes the subset of the $L = N(N-1)/2$ active links experiencing a sufficiently high signal strength to support reliable communication. The two links associated with the same pair of WSs are assumed to be reciprocal. At any time t the AP collects a set of L noisy measurements $\mathbf{s}_t = [s_{\ell,t}]_{\ell \in \mathcal{L}}$ where each observation $s_{\ell,t}$ represents the power of the RSS measured over the $\ell \in \mathcal{L}$ link. As depicted in Fig. 2 and detailed in Sect. II-A, measurements are collected in real-time based on a proprietary MAC protocol defined on top of the IEEE 802.15.4 standard that allows a periodic transmission of *probe signals* by all the N sensors over reserved time-slots.

We assume that one[1] object might move inside the detection region $\mathcal{X}$. The object does not need to carry any electronic device and it is not aware of being localized. At discrete time instant $t = 1, \ldots, T$, with time sampling interval Δt, the position of the object being detected is indicated by coordinates $\mathbf{x}_t = [x_{1,t}, x_{2,t}] \in \mathcal{X}$. Based on the observations $\mathbf{s}_t$ available at the AP, the problem we tackle is to localize[2] at each time instant t the object within the region $\mathcal{X}$, i.e. to estimate the position $\mathbf{x}_t$ given the available measurements up to time t. The object position $\mathbf{x}_t$ is not directly observable but it is hidden into the noisy RSS measurements $\mathbf{s}_t$ according to the statistical model defined in Sect. II-B.

A. Network Architecture and Protocols for Radio Imaging

The radio imaging system has stricter reliability and delay requirements compared to conventional WSN applications. Each sensor must sample the RSS field at constant sampling rate $1/\Delta t$. The real-time constraint prescribes that the whole observation data-set $\mathbf{s}_t$ should be decoded and processed by the AP before a new data set $\mathbf{s}_{t+1}$ is generated after Δt sec. This hard deadline calls for the development of advanced wireless link-layer management policies.

The proposed MAC sub-layer uses a timed-token passing protocol [5] on top of the cooperative network architecture illustrated in Fig. 2. Medium access is based on time division while token message exchange (dashed black arrow) is used to periodically synchronize the network. When the sensor receives the token message it is configured to perform two tasks: *i)* transmit the backlog of RSS measurements over a default IEEE 802.15.4 channel used for communication with the AP (red arrow) over center frequency f_c; *ii)* broadcast the probe signal (solid arrow) over a pre-configured channel at center frequency $f_m \neq f_c$. During MAC configuration the sensor network is organized into a logical ring connecting the WSs within the detection area to the AP (and viceversa). To enforce the real-time constraint, still guaranteeing the service reliability, error control is based on implicit acknolwedgements: each sensor is configured to wait for the token message until a time-to-token-visit listening time expires, after that it is allowed to generate a new token and to exclude the links with poor quality.

B. RSS Measurement Model

This section presents a stochastic model that relates the noisy power observation $\mathbf{s}_t$ to the target position $\mathbf{x}_t$. The model has been corroborated by an experimental analysis outlined in Sect. IV. The RSS measured over link ℓ in dBm is modelled as a Gaussian random variable whose parameters depend on the absence (indicated as $\mathbf{x}_t = \mathbf{0}$) or presence ($\mathbf{x}_t \in \mathcal{X}$) of a target in the detection area and, in case of presence, on the specific position $\mathbf{x}_t$ within $\mathcal{X}$:

$$s_{\ell,t} = \begin{cases} h_\ell(\mathbf{0}) + w_\ell(\mathbf{0}), & \text{if } \mathbf{x}_t = \mathbf{0} \\ h_\ell(\mathbf{x}_t) + w_\ell(\mathbf{x}_t), & \text{if } \mathbf{x}_t \in \mathcal{X} \end{cases} \quad (1)$$

In case of missing target, the link ℓ experiences an average received power $h_\ell(\mathbf{0})$ that accounts for the propagation effects due to fixed obstructions as metallic reflectors, walls and floor. On the other hand, the Gaussian noise $w_\ell(\mathbf{0}) \sim \mathcal{N}(0, \sigma^2_\ell(\mathbf{0}))$, with zero mean and standard deviation $\sigma_\ell(\mathbf{0})$, models the randomness of shadowing due to variations (typically moderate) in the surrounding environment, such as objects or people moving outside the detection area. When a target enters the WSN area, both the average attenuation $h_\ell(\mathbf{x}_t)$ and the fading $w_\ell(\mathbf{x}_t) \sim \mathcal{N}(0, \sigma^2_\ell(\mathbf{x}_t))$ are affected in a way that depends on the position $\mathbf{x}_t$. As also confirmed experimentally in [4], if $\mathbf{x}_t$ is along the link ℓ, the signal typically experiences an increased path-loss $h_\ell(\mathbf{x}_t)$. In addition, an increased fluctuation around the average is also observed as the target moves, turns, etc. in the surrounding of the point $\mathbf{x}_t$.

Both the path-loss and the random fading provide significant information on the target location. This can be easily seen by the experimental 2D functions (or maps) $h_\ell(\mathbf{x}_t)$ and $\sigma_\ell(\mathbf{x}_t)$ shown in Fig. 3 obtained as detailed in Sect. IV. Measurements show that the presence of a moving person in the coverage area of the WSN induce significant fades on the power of signals exchanged by the nodes of the WSN. Fading effects, however, are difficult to classify in complex indoor scenarios (for outdoor studies, see, e.g. the analysis of the power changes due to wind-blown foliage [6]). Hence, for the indoor case study here considered, we choose to evaluate the model functions $h_\ell(\mathbf{x}_t)$ and $\sigma_\ell(\mathbf{x}_t)$ through experimental power maps measured by the WSN during a preliminary off-line calibration phase over relevant set-points $\mathbf{x}_t$.

[1] Extension to multiple nodes is out of the scope of this paper.

[2] Detection problem reduces to identify any relevant change in the observations and it is not treated here.

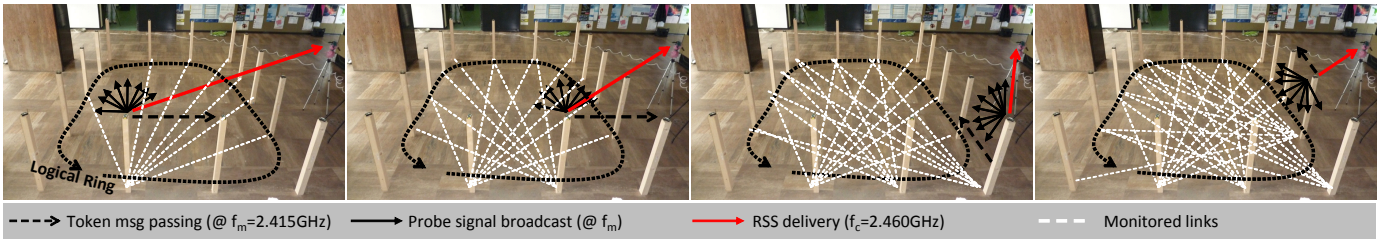

Fig. 2. Cooperative network architecture for Radio Imaging: timed-token message passing.

Thereby, the target detection and tracking procedure is carried out by following two steps:

1. Trajectory-based calibration: an object (with similar characteristics of the intended target) moves according to a known training trajectory that spans M different positions $\{\mathbf{u}_m\}_{m=1}^{M} \in \mathcal{X}$; the AP collects and synchronizes the RSS observations received from the sensors while these are used to evaluate a sample average $h_\ell(\mathbf{u}_m)$ and a sample standard deviation $\sigma_\ell(\mathbf{u}_m)$ for each link.

2. On-line localization and tracking: at each time instant t, each sensor periodically measures and forwards the RSS of active links. The AP receives the data set $\mathbf{s}_t$, and this is used for detection and on-line estimation of the object position $\hat{\mathbf{x}}_t$ based on the knowledge of the 2D maps.

III. Positioning Algorithms

In this section, we introduce the Bayesian framework for on-line sequential estimation of the object trajectory $\mathbf{x}_{1:T} = [\mathbf{x}_1 \cdots \mathbf{x}_T]$ from the observations $\mathbf{s}_{1:T} = [\mathbf{s}_1 \cdots \mathbf{s}_T]$.

The target motion is modeled as a first-order Hidden Markov Model (HMM), described by the system equation $\mathbf{x}_t = \mathbf{x}_{t-1} + \mathbf{v}_t$, where $\mathbf{v}_t$ denotes the driving process with known distribution $f_{\mathbf{v}}(\mathbf{v})$. Transition probabilities are given by $p(\mathbf{x}_t|\mathbf{x}_{t-1}) = f_{\mathbf{v}}(\mathbf{x}_t - \mathbf{x}_{t-1})$. The initial state distribution $p(\mathbf{x}_1)$, for any $\mathbf{x}_1 \in \mathcal{X}$, is chosen based on the available a-priori information about the target object position at time $t = 1$: it can be either uniform in case of missing a-priori information (detection problem) or impulsive in case of knowledge of the starting location.

The state $\mathbf{x}_t \in \mathcal{X}$ is hidden into the observation $\mathbf{s}_t \in \mathbb{R}^L$. Observations $s_{\ell,t}$ are assumed to be conditionally independent over ℓ given the state $\mathbf{x}_t$. Recalling the model (1), the measurement $\mathbf{s}_t$ conditioned to $\mathbf{x}_t$ is an uncorrelated Gaussian vector with mean $\mathbf{h}(\mathbf{x}_t) = [h_\ell(\mathbf{x}_t)]_{\ell\in\mathcal{L}}$ and covariance $\mathbf{C}(\mathbf{x}_t) = \mathrm{diag}\left([\sigma^2_\ell(\mathbf{x}_t)]_{\ell\in\mathcal{L}}\right)$. Thus, the conditioned distribution is:

$$p(\mathbf{s}_t|\mathbf{x}_t) = \frac{1}{(2\pi)^{L/2}|\mathbf{C}(\mathbf{x}_t)|^{1/2}} \exp\left\{-\frac{1}{2}\|\mathbf{s}_t - \mathbf{h}(\mathbf{x}_t)\|^2_{\mathbf{C}^{-1}(\mathbf{x}_t)}\right\} \quad (2)$$

where $\|\mathbf{s}\|^2_{\mathbf{C}} = \mathbf{s}^{\mathrm{T}}\mathbf{C}\,\mathbf{s}$ denotes the square norm of the vector $\mathbf{s}$ weighted by the matrix $\mathbf{C}$.

A local estimate of $\mathbf{x}_t$ can be obtained by applying the MLE criterion on the measure $\mathbf{s}_t$ only: $\hat{\mathbf{x}}_t = \arg\max_{\mathbf{x}_t\in\mathcal{X}} p(\mathbf{s}_t|\mathbf{x}_t)$. A Bayesian approach is proposed to exploit the a-priori information on the target mobility and improve the estimate performance; the a-posteriori probability density function (pdf), $p(\mathbf{x}_t|\mathbf{s}_{1:t})$, of the state given the whole measurement set $\mathbf{s}_{1:t} = [\mathbf{s}_1 \cdots \mathbf{s}_t]$, is obtained recursively according to [7]:

$$p(\mathbf{x}_t|\mathbf{s}_{1:t}) \propto p(\mathbf{s}_t|\mathbf{x}_t) \underbrace{\int_{\mathcal{X}} p(\mathbf{x}_t|\mathbf{x}_{t-1}) p(\mathbf{x}_{t-1}|\mathbf{s}_{1:t-1}) d\mathbf{x}_{t-1}}_{p(\mathbf{x}_t|\mathbf{s}_{1:t-1})}, \quad (3)$$

where constant terms have been neglected. The a-priori pdf $p(\mathbf{x}_t|\mathbf{s}_{1:t-1})$ is obtained from the a-posteriori pdf of the previous step $p(\mathbf{x}_{t-1}|\mathbf{s}_{1:t-1})$ and the knowledge of the transition probabilities $p(\mathbf{x}_t|\mathbf{x}_{t-1})$ for any $t > 1$, while it is initialized with $p(\mathbf{x}_t|\mathbf{s}_{1:t-1}) = p(\mathbf{x}_1)$ for $t = 1$. Once the a-posteriori pdf is calculated using (3), the estimate of the state $\mathbf{x}_t$ can be obtained using either the maximum-a-posteriori (MAP) $\hat{\mathbf{x}}_t = \arg\max_{\mathbf{x}_t\in\mathcal{X}} p(\mathbf{x}_t|\mathbf{s}_{1:t})$ or the minimum mean square error (MMSE) criterion $\hat{\mathbf{x}}_t = \int_{\mathcal{X}} \mathbf{x}_t p(\mathbf{x}_t|\mathbf{s}_{1:t}) d\mathbf{x}_t$.

The grid-based approach [8] here used for the implementation of (3) relies on a uniform 2D sampling of the continuous state space $\mathcal{X}$. The target object location $\mathbf{x}_t$ is thus assumed to take values within a regular 2D grid of $K = K_1 K_2$ spatial positions, $\mathbf{k}\Delta x = [k_1, k_2]\Delta x$, with sampling interval Δx, $k_1 = 1, \ldots, K_1$ and $k_2 = 1, \ldots, K_2$. A-priori pdf $p(\mathbf{x}_t|\mathbf{s}_{1:t-1})$ in (3) is thus approximated by a finite sum.

IV. Experimental Study

In the proposed experimental set-up, protocols to enable radio imaging are implemented over battery-powered Micaz Motes based on the low-power single-chip 2.4 GHz IEEE 802.15.4 compliant device CC2420 [9]. As depicted in Fig. 3 (top-left corner), $N = 14$ nodes are regularly deployed in an open-space room along the boundary of a rectangular indoor area of size 5m×4m. The target is a person moving inside the detection area. The 8-bit RSS indicator (RSSI) is used to measure the RSS, here ranging between −90dBm and −30dBm. Radio transmit power is set to 0dBm. The RSS sampling time interval Δt needs to be adapted to the target mobility model. Assuming that the target velocity is below 1m/s, here the sampling interval is set to $\Delta t = 120$ms. The AP node collecting data from sensors is implemented over a Telosb Mote equipped with Texas Instruments MSP430 microcontroller. Measurements are sent to a PC for data processing and imaging.

A. Model Calibration and Validation

During the calibration phase, a person moves along a known training trajectory of $M = 35$ positions $\{\mathbf{u}_m\}_{m=1}^{M}$ as indicated

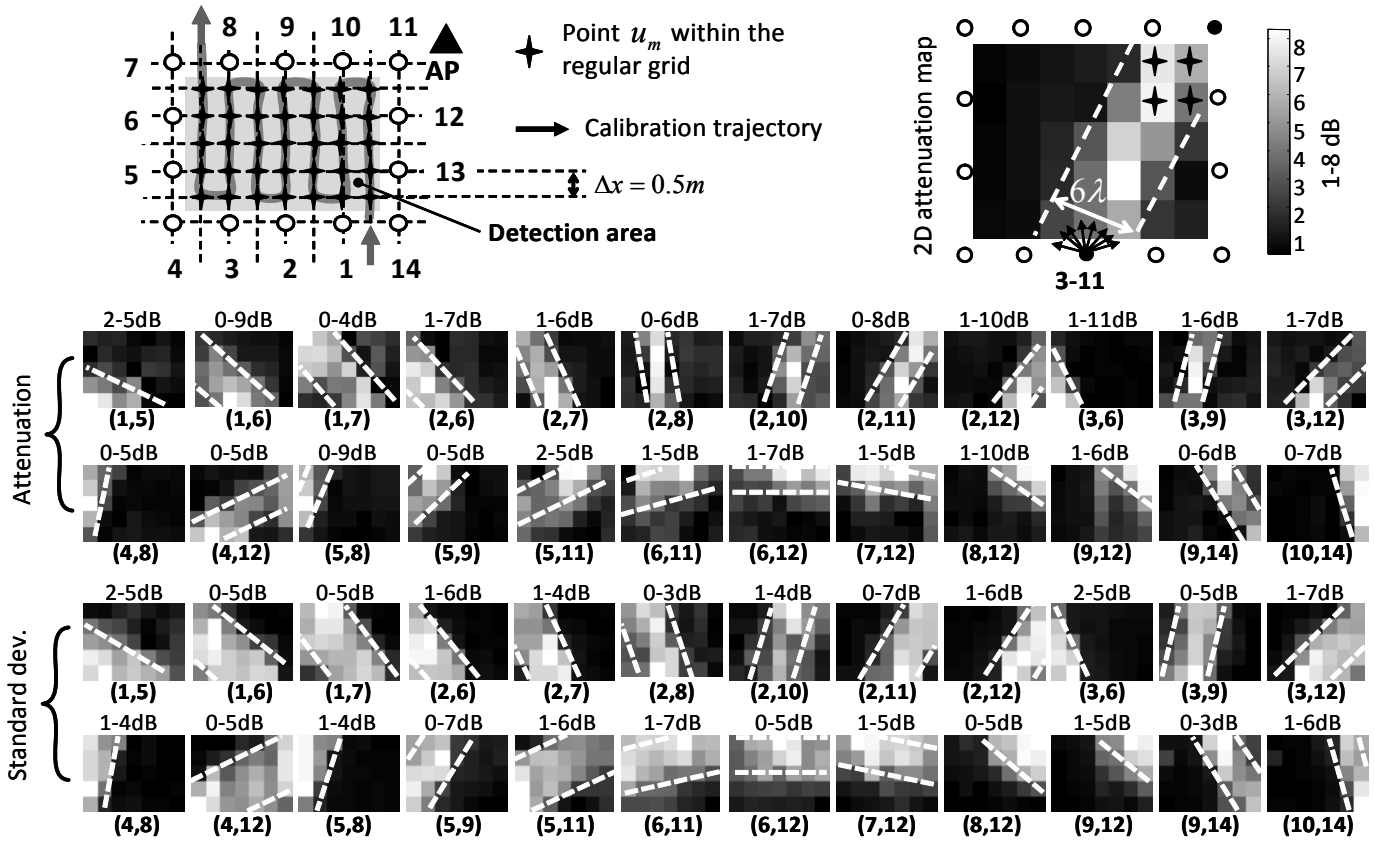

Fig. 3. Top-left corner sub-figure: WSN layout for the indoor tests. Top-right corner sub-figure: example of 2D attenuation map for link 3-11 and strip model. Bottom sub-figures: examples of 2D attenuation and standard deviation maps for selected links.

in Fig. 3 (top left corner) with a velocity of approximately 1m/s, yielding 8 RSS samples per position on average. The trajectory covers all the $K = 7 \times 5$ locations of the 2D regular grid used for approximating the state space $\mathcal{X}$, with spatial sampling interval $\Delta x = 0.5$m. In Fig. 3, the 2D maps for attenuation $h_\ell(\mathbf{x}_t)$ and standard deviation $\sigma_\ell(\mathbf{x}_t)$ calculated from the RSS measurements gathered along the training trajectory are shown for a selected subset of links $\ell = (i, j)$, with nodes $i = 1, ..., N$ and $j = 1, ..., N$ numbered as in the top-left corner sub-figure. The 2D maps provide a statistical description of the change in attenuation and standard deviation caused by the moving target. For illustrative purpose, a detailed view of the attenuation map for link $(3, 11)$ is reported in the top-right corner of Fig. 3. Each pixel of the map represents the difference $h_\ell(\mathbf{0}) - h_\ell(\mathbf{x}_t)$ in gray scale, i.e. the increase of path-loss (in dB) experienced over the link ℓ when the target is on position $\mathbf{x}_t$ compared to the case of no target. The white/gray region where the target generates a significant path-loss (2-10dB), is shaped as a strip of width $6 \div 7\lambda$ centered around the direct path connecting the two nodes, $\lambda = 0.125$m being the carrier wavelength. In the figure, this sensitivity strip is highlighted by two white dashed lines delimiting the region and it is indicated as $\mathcal{X}_\ell^{(a)} \subset \mathcal{X}$ for link ℓ. A similar reasoning holds for the shadowing standard deviation increase, $\sigma_\ell(\mathbf{x}_t) - \sigma_\ell(\mathbf{0})$, as shown by the maps at the bottom of the figure. For any link ℓ the strip $\mathcal{X}_\ell^{(s)}$ defines the locations where a significant change in the standard deviation could be observed due to the target presence. Compared to the attenuation, the strip width is larger, approximately $8 \div 9\lambda$, and the increase of standard deviation ranges between 1-7dB. By looking at the 2D maps in Fig. 3, it is reasonable to conclude that the *joint* exploitation of attenuation and standard deviation maps can provide a significant amount of information for accurate mobile positioning. Optimal combination of these two observations for all links in the likelihood evaluation allows to turn the measurement uncertainty (i.e., the noise $w_\ell(\mathbf{x}_t)$) into an advantage by exploiting the variation of the degree of uncertainty (i.e., $\sigma_\ell(\mathbf{x}_t)$) over the space as a useful information for location estimation, which is especially important in case of high shadowing effects. This occurs mainly in complex propagation environments with non line-of-sight links where the effect of target obstruction is expected to be more relevant and thus changes in RSS standard deviation likely provide more information for localization than the attenuation.

Long-term changes of the propagation and interference environment constrain the adoption of an automatic procedure to periodically update the model parameters. Looking at the 2D maps in Fig. 3, the most significant information for parameter estimation is confined inside each strip where moving objects cause significant RSS fluctuations and is typically represented by the increase of attenuation/standard-deviation (strip width may be assumed constant). Therefore, it is reasonable to define a decision-directed approach for model adjustment during on-

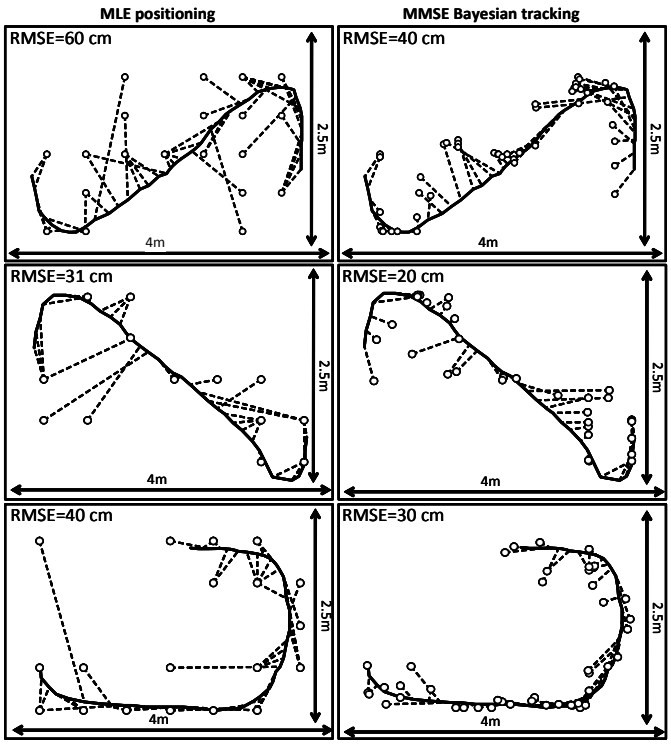

Fig. 4. Examples of trajectories (solid lines) and relative estimation (markers) with MLE and MMSE Bayesian tracking. Dashed lines connecting the true and the estimated positions highlight the localization errors while root mean squared error (RMSE) is indicated for each case.

line imaging: any the new observation $\mathbf{s}_t$ indicating a target at position $\hat{\mathbf{x}}_t \in \mathcal{X}_\ell^{(a)}$ (or $\hat{\mathbf{x}}_t \in \mathcal{X}_\ell^{(s)}$ for standard deviation) can be used to update on-line the value of the attenuation (or standard deviation) along the link-ℓ sensitivity region.

B. Mobile Positioning Performance

Fig. 4 shows some tracking examples selected from the indoor tests. The figure compares the true target trajectories acquired using a video-camera (solid line) with the estimated ones (markers) obtained by MLE estimate (left side sub-figures) and MMSE Bayesian tracking (right side sub-figures). Position estimate is updated on every $\Delta t = 120$ms: this allows to jointly process one RSS sample per link. The localization errors can be appreciated by looking at the dashed lines that connect the true and the estimated positions. The root mean squared error (RMSE) is also indicated for each case. The MLE performance is affected by false-localization problems distributed over all the detection area causing localization errors up to 2.5m. A main limiting factor for the local MLE is the spatial accuracy of pairwise location measurements, in other words, the sensitivity strip width. The Bayesian tracking algorithm reduces the average error below 0.5m. Notice that higher performance might be obtained by particle filtering.

In Fig. 5 we compare the image results for MLE estimation and Bayesian tracking given that one human is standing in three different positions indicated by markers inside the detection area. Images represent the likelihood function $p(\mathbf{s}_t|\mathbf{x}_t)$ for MLE estimation and the a-posteriori pdf $p(\mathbf{x}_t|\mathbf{s}_{1:t})$ for

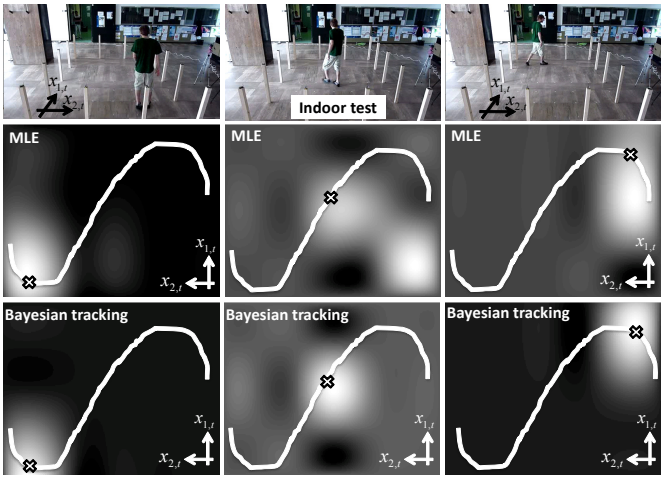

Fig. 5. Top: indoor test environment with human moving along an arbitrary trajectory. Bottom: image results for MLE estimation and Bayesian tracking representing the likelihood function $p(\mathbf{s}_t|\mathbf{x}_t)$ and the a-posteriori pdf $p(\mathbf{x}_t|\mathbf{s}_{1:t})$, respectively, for positions $\mathbf{x}_t \in \mathcal{X}$ corresponding to top sub-figures.

Bayesian tracking over the regular grid of states $\mathbf{x}_t \in \mathcal{X}$. Image artifacts observed by MLE estimation can be removed by Bayesian filtering thus improving positioning accuracy.

V. Concluding Remarks

Radio imaging can be used to locate and track moving objects or people in areas with a low-cost cooperative wireless network operating at RF wavelengths. A log-normal RSS model describes the fading effects caused by object/human movement in indoor environments; this allows to cast the imaging problem into the framework of Bayesian filtering. The use of the Bayesian tracking approach is shown to provide a reasonable accuracy for target localization and it is expected to provide an effective solution ready for a wide range of industrial applications.

References

[1] N. Patwari, et al., "Locating the nodes: cooperative localization in wireless sensor networks," IEEE Signal Processing Mag., Vol. 22, No. 4, pp. 54-69, July 2005.

[2] M. Youssef, M. Mah, A. Agrawala, "Challenges: device-free passive localization for wireless environments," Proc. of ACM-MobiCom Montreal, Canada, Sept. 2007.

[3] S. Gezici et al., "Localization via ultra-wideband radios: a look at positioning aspects for future sensor networks," IEEE Signal Processing Mag., vol. 22, pp. 70–84, July 2005.

[4] J. Wilson, N. Patwari, "Radio tomographic imaging with wireless networks" IEEE Trans. on Mobile Comp., vol. 9 no. 5, May 2010.

[5] E. Tovar, F. Vasques, "Real-time fieldbus communications using Profibus networks," IEEE Trans. on Industrial Electronics, vol. 46, no.6, pp.1241-1251, Dec. 1999.

[6] P. K. Chong, et al., "Wind-blown foliage and human induced fading in ground-surface narrowband communications," IEEE Trans. on Vehicular Technology, vol. 60, no. 4, May 2011.

[7] M. S. Arulampalam, et al. "A tutorial on particle filters for online nonlinear/non-Gaussian Bayesian tracking," IEEE Trans. Signal Proc., Vol. 50, No. 2, Feb. 2002.

[8] M. Nicoli, C. Morelli, V. Rampa, "A jump Markov particle filter for localization of moving terminals in multipath indoor scenarios," IEEE Trans. Signal Processing, vol. 56, n. 8, August 2008.

[9] Datasheet CC2420, 2.4 GHz IEEE 802.15.4 ZigBee-ready RF Transceiver, Mar. 2007.